YALE PEABODY MUSEUM

JOURNAL OF MARINE RESEARCH

The *Journal of Marine Research,* one of the oldest journals in American marine science, published important peer-reviewed original research on a broad array of topics in physical, biological, and chemical oceanography vital to the academic oceanographic community in the long and rich tradition of the Sears Foundation for Marine Research at Yale University.

An archive of all issues from 1937 to 2021 (Volume 1–79) are available through EliScholar, a digital platform for scholarly publishing provided by Yale University Library at https://elischolar.library.yale.edu/.

Requests for permission to clear rights for use of this content should be directed to the authors, their estates, or other representatives. The *Journal of Marine Research* has no contact information beyond the affiliations listed in the published articles. We ask that you provide attribution to the *Journal of Marine Research.*

Yale University provides access to these materials for educational and research purposes only. Copyright or other proprietary rights to content contained in this document may be held by individuals or entities other than, or in addition to, Yale University. You are solely responsible for determining the ownership of the copyright, and for obtaining permission for your intended use. Yale University makes no warranty that your distribution, reproduction, or other use of these materials will not infringe the rights of third parties.

Seabed drag coefficient over natural beds of horse mussels (*Atrina zelandica*)

by Malcolm O. Green[1], Judi E. Hewitt[1] and Simon F. Thrush[1]

ABSTRACT

Measurements of seabed drag coefficient, C_{100}, were made under tidal currents at four sites in Mahurangi Harbour, New Zealand. At the first three sites the dominant roughness element was the pinnid bivalve, *Atrina zelandica* (horse mussel). At the fourth site, which was devoid of horse mussels but covered in cockle shells, patches of seaweed and crab burrows, C_{100} was smallest (0.0055), but still twice as large as the value typically applied to abiotic, flat, cohesionless seabeds (0.0025). The mean drag coefficient plus-or-minus standard error at the three sites with horse mussels was: 0.0082 ± 0.0010 (site 1); 0.0096 ± 0.0009 (site 2); 0.0115 ± 0.0016 (site 3). There were no clear differences amongst sites 1, 2 and 3 in terms of the attributes of individual horse mussels (e.g. shell height, width or orientation), which could have been used to explain the ranking of the drag coefficients. There were, however, differences amongst the three sites in terms of spatial distribution of individual bivalves. The site with the highest density of horse mussels, site 1, had the lowest drag coefficient and an areal concentration (λ) of horse mussels higher than typical values cited for the critical concentration (λ_c) for the onset of skimming flow over various idealized, three-dimensional roughness elements. At sites 2 and 3, the drag coefficient was given by:

$$C_{100} = \left[\frac{\kappa}{\ln (3000/mk\lambda)} \right]^2$$

which was valid for $\lambda < \lambda_c$, where κ is von Karman's constant, k is the horse mussel height (i.e., protrusion above the seabed), $m \approx 100$ and $\lambda_c \approx 0.2$. The stable eddies that are hypothesized to lodge between roughness elements at concentrations greater than λ_c may influence benthic community dynamics.

1. Introduction

The seabed drag coefficient, C_{100}, reflects the proportion of mean-flow kinetic energy dissipated in the benthic boundary layer by turbulence. Although the flow-circulation modeler typically treats the drag coefficient as a box in which errors are accumulated in order to calibrate circulation models, the drag coefficient is nevertheless a real link between flow kinematics and dynamics. As such, its actual value has meaning for those, such as sediment dynamicists and benthic ecologists, who need to understand frictional forces

---

1. NIWA, National Institute of Water and Atmospheric Research, P.O. Box 11-115, Hamilton, New Zealand.

generated by water flowing over the seabed and the consequences of friction to sediment entrainment and benthic community dynamics, respectively.

In clear, rough-turbulent, steady flow, the size of C_{100} is governed by the roughness of the seabed, which is usually equated with the sediment texture if there are no bedforms or, if there are bedforms, with the bedforms' size and shape. The basic relationship between hydraulic roughness (which is related to C_{100}—see Eq. (4.4) below) and boundary geometry was derived by Wooding *et al.* (1973) and Yaglom (1979). Soulsby (1990) and Whitehouse and Chesher (1994) have reviewed investigations of steady-flow roughness attributable to bedforms and sediment texture, including the early work of Sternberg (1968 and 1970) and Kamphuis (1974). Dyer (1980) and Wilkinson (1986) observed large temporal variation in hydraulic roughness in estuaries, and Soulsby (1990) reported the effect of bedform orientation on hydraulic roughness. Smith and McLean's (1977) work on roughness of superimposed bedforms has proven to be seminal. Hydraulic roughness due to near-bed granular saltation was formulated by Dietrich (1982) and Wiberg and Rubin (1989). Green and McCave (1995) interpreted measurements of C_{100} under tidal flows in a shallow sea in terms of stratification of the boundary-layer flow by suspended sediment. Hydraulic roughness of loose sand beds under waves was investigated by Grant and Madsen (1982) and Nielsen (1983), and the enhancement of drag by nonlinear interaction between waves and currents in the boundary layer was formulated initially by Grant and Madsen (1979) and later verified using field data by Grant *et al.* (1984), Huntley and Hazen (1988) and Green *et al.* (1990).

The above literature deals with abiotic seabeds, but in many places the seabed is grossly modified by benthic biota. That is the case in northern New Zealand estuarine and inner-shelf waters, where the pinnid bivalve *Atrina zelandica* (horse mussel) frequently dominates the seabed landscape. Observations by divers and side-scan sonar have revealed large (100-m spatial scale) patches of horse mussels carpeting the seafloor, which have the potential to modify boundary-layer dynamics and sediment transport. Conversely, changes in boundary-layer dynamics induced by biogenic roughness may affect the ecology of the reef-forming organism and associated communities (e.g., Warwick *et al.,* 1997; Cummings *et al.,* 1998).

There are three ways seabed roughness can be altered biologically: surface roughness can be altered by biogenic structures (e.g., burrows and tubes); animals themselves can act as roughness elements; bulk sediment characteristics can be altered through, for instance, adhesion (Rhoads and Boyer, 1982; Nowell *et al.,* 1981; Grant *et al.,* 1982). Despite its potential importance, compared to abiotic seabeds there have been fewer measurements of the structure of the boundary layer over natural biogenic features in coastal and estuarine waters (Grant and Madsen, 1986). Chriss and Caldwell (1982) explained the existence of segmented velocity profiles by two different roughness scales attributable to biologically generated bedforms on a muddy seabed, and Cacchione *et al.* (1983) have described how muddy-seabed microtopography and roughness are controlled by benthic biota on the continental shelf. The STRESS project has yielded observations of the temporal variability

of bed configuration in the mid-shelf silt belt and the contribution made to that variability by biogenic influences (e.g., Wheatcroft, 1994). There is a body of work addressing the role of the boundary-layer flow in maintaining concentration boundary layers above beds of the blue mussel (e.g., Frechette *et al.,* 1989; Butman *et al.,* 1994), and small-scale field studies and flume experiments have documented flow around individual and model biological features (e.g., Eckman *et al.,* 1981; Eckman, 1985; O'Riordan *et al.,* 1993). Flow dynamics is strongly conditioned by seagrass and macroalgal beds, which can affect benthic community structure (Peterson *et al.,* 1984) and enhance deposition of suspended material (Madsen and Warnke, 1983). Gambi *et al.* (1990) investigated flow dynamics associated with eelgrass beds, and found two-layer flow with high shear stress at the canopy-water interface and reduced turbulence in the below-canopy habitat. At yet smaller scales, Hurd *et al.* (1997) visualized flow around individual blades of giant kelp and inferred the thickness of the diffusion boundary layer. Shashar *et al.* (1996) investigated boundary-layer structure at several scales on a coral reef.

We describe here an experiment aimed at measuring C_{100} over beds of horse mussels in tidal currents in a northern New Zealand estuary. Our objective is to relate the measured value of C_{100} to a quantitative description of horse mussel population at each of several sites. The results demonstrate a link between ''mesoscale'' (order 100 m) patchiness of the benthic biota and flow dynamics, and extend knowledge of drag coefficients beyond that relating to abiotic seabeds.

2. Location

The data are from Mahurangi Harbour, a small estuary (25 km²) on the east coast of the North Island of New Zealand, approximately 50 km north of Auckland (Fig. 1). All measurements were made over one week in the lower estuary, where there are extensive beds of horse mussels. Sand flats flank the main channel and emerge at low tide. The tidal range in the lower estuary varies from 1.4 m at neaps to 3.1 m at springs; the data were collected during spring tides. Circulation is dominated by the semi-diurnal tide and the water column is typically well mixed, although stratification of the upper estuary does occur after heavy rain. Tidal streams in the lower estuary attain maximum speeds of ~50 cm/s at 100 cm above the bed. The estuary is quite sheltered from ocean swell by virtue of the mouth's orientation and the presence of offshore islands.

3. Site selection and data acquisition

Past side scan sonar surveys and diver observations of Mahurangi Harbour were drawn upon to map horse mussel patches in the estuary. Four experimental sites (Fig. 1; Table 1) that together spanned the greatest possible range of seabed roughness were chosen. Each site was located approximately in the middle of an area of homogeneous seabed that stretched for at least 300 m in a direction parallel to the principal tidal axis, and there was a shallow submerged reef 100 m beyond site 3 in the up-estuary direction. An ''L''-shaped
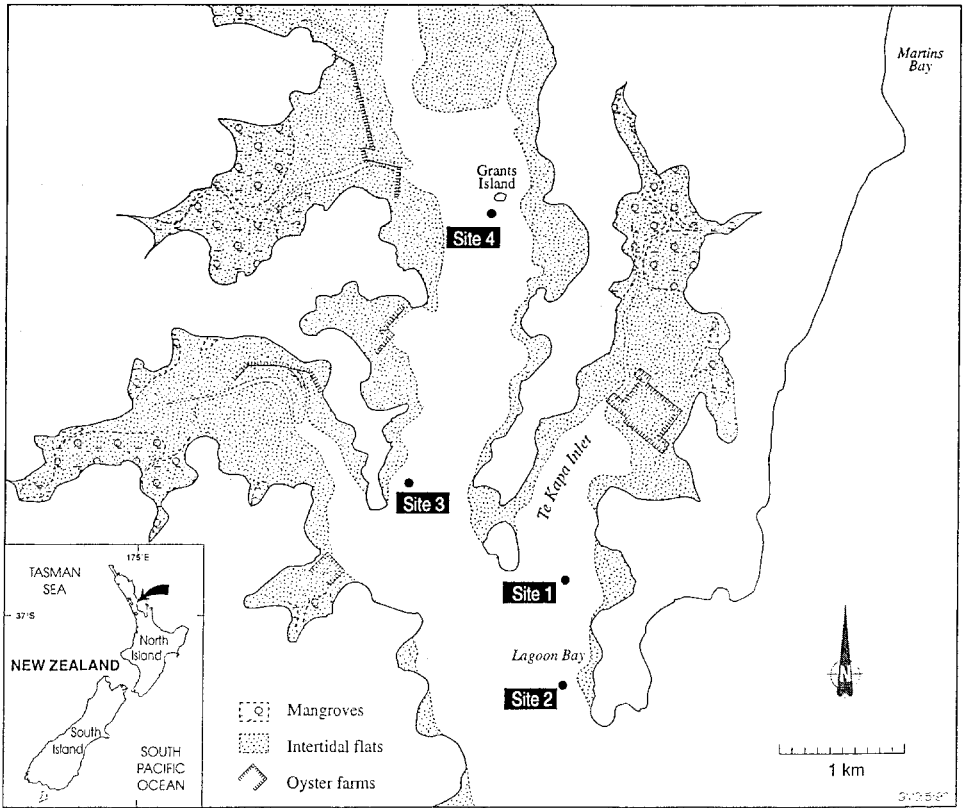
Figure 1. Location map.

transect was laid out at each site for measuring seabed roughness, and a seabed-mounted instrument array was deployed at each site for measuring currents. The transect in each case was situated within 20 m of the instrument array, but transect observations were not necessarily conducted at exactly the same time as currents were measured. Current measurements acquired at site 3 during ebb flows are discarded from the following analysis, as currents in that case were contaminated by wakes shed from the up-estuary reef.

Video observations were made at each site along two 20-m transects that were laid out with rope pegged to the seabed and marked at 50-cm intervals. One transect was aligned with the principal axis of the tidal current and the other crossed that axis at right angles to form an "L" shape. The video camera was carried by a diver, who held the camera vertically at constant elevation above the bed. The diver used a ruler to measure the height (i.e., protusion above the seabed) of 10 randomly selected horse mussels along each transect. The diver was also prepared to measure bedform geometry; however, there were no bedforms at any site.

At each site, current velocity was measured at four elevations above the bed using an

Table 1. Site details. D_g is the mean grain size of the bed sediment, which was determined from analysis of a seabed sample taken at each site. A Mastersizer laser system was used to measure the grainsize distribution in 0.5-phi intervals over a range of -1 to 14.5 phi. The characterization of the seabed roughness is expanded and explained in subsequent text and in Table 2; z_r is the reference elevation; see the text for details. The depth is relative to MSL.

Site	Sediment	Dominant feature of seabed roughness	z_r (cm)	Depth (m)
1 (Te Kapa)	muddy-sandy, $D_g = 120 \mu m$	horse mussels	24	4
2 (Lagoon Bay)	sandy-shelly, $D_g = 130 \mu m$	horse mussels	16	5
3 (Mid-Harbour)	muddy, $D_g = 90 \mu m$	horse mussels	22	3
4 (Grants Island)	muddy, $D_g = 14/80 \mu m$ (bimodal)	crab burrows; patches of dead cockles (*Austrovenus stutch-buryi*) and seaweed (*Graciaria* sp.)	16	3

array of Marsh-McBirney electromagnetic current meters (3.8-cm diameter spherical head) mounted on a self-contained tripod (''ALICE''). Currents were measured for 8.53 min every half hour for approximately 25 h (two complete tidal cycles). The sampling interval was 0.25 s (2048 points per burst). Pressure was measured concurrently with a Paroscientific quartz pressure sensor located 1.2 m above the bed. The current meters were located at elevations above the bed (z) of $z_r + 0$, $z_r + 33$, $z_r + 82$ and $z_r + 146$ cm, where z_r is a reference elevation that varied slightly from site to site (Table 1). The reference elevation is effectively the elevation above the bed of the lowest current meter, which was measured at each site by divers as the distance between the mid-point of the lowest current meter and the top of the seabed immediately below the current-meter array. Where there were horse mussels, z_r is defined as the distance between the mid-point of the lowest current meter and the point halfway between the seabed surface and the top of the mussels.

The current meters were attached to the tripod by a series of cantilevers (Fig. 2). In order to minimize contamination of the current data by wakes shed from the hardware, ALICE was oriented on the seabed at each site such that the instrument array pointed across the principal axis of the tidal stream. Nevertheless, there was a problem with contamination of the flow by wakes that only became evident after the experiment and that necessitated using current data from only three levels. With the mean flow impinging on the current meters from the right (looking from the center of the tripod outwards; Fig. 2), data from the top current meter had to be discarded, and with the mean flow impinging from the left, data from the next current meter down had to be discarded.

4. Data analysis

a. Flow measurements

Current-meter zero offsets (units: cm/s) were determined by still-water bucket test conducted before and after the experiment. Current meter gains (units: cm/[s*volt]) supplied by the instrument manufacturer were verified using 6 hours (twelve 8.53-min
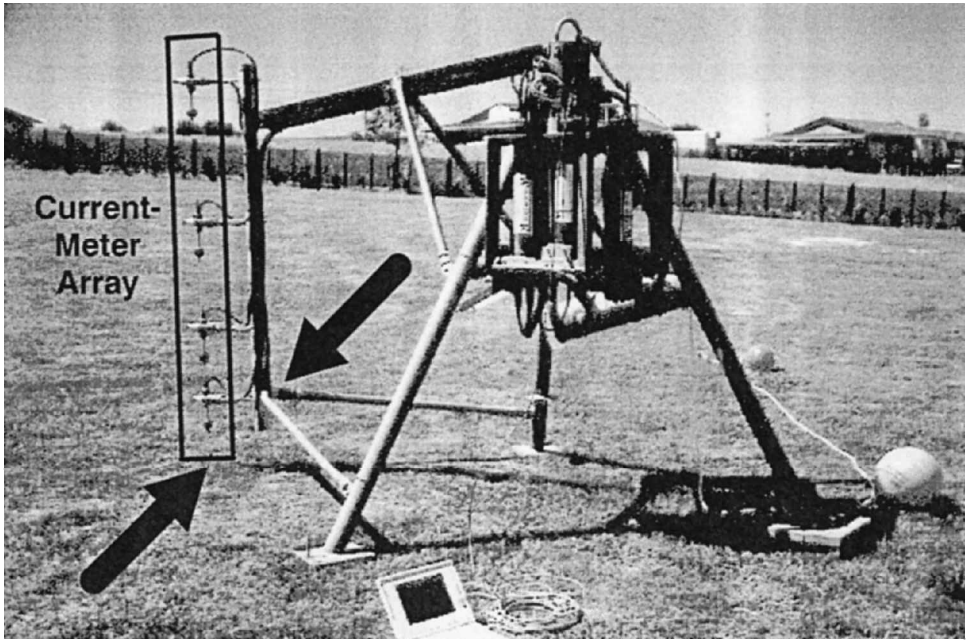
Figure 2. The instrumented tripod ALICE showing the current-meter array and the way ALICE was aligned relative to the tidal current to achieve minimum contamination of flow data by wakes shed from the hardware. Thick arrows represent the principal axis of the tidal stream.

bursts) of test data obtained from shallow water at Martins Bay, on the open coast (Fig. 1), where steady flows were negligible and gravity-wave-orbital motions were dominant. The verification consisted of comparing u_w with $u_{w,\text{linear}}$, as follows. u_w is the measured wave-orbital-speed standard deviation, which was calculated from each burst of current-meter data as:

$$u_w = \sqrt{\int_{1/2}^{1/30} \varepsilon(f)df} \tag{4.1}$$

where $\varepsilon(f)$ is the power spectrum of the measured current speed, f is frequency and the limits of integration correspond to the gravity-wave range of frequencies. $u_{w,\text{linear}}$ is the wave-orbital-speed standard deviation at the level of a given current meter (z_u), predicted from the pressure data using linear wave theory as:

$$u_{w,\text{linear}} = \frac{2\pi h_{\text{SD}} \cosh(k_w \overline{h}) \cosh(k_w z_u)}{\overline{T} \sinh(k_w \overline{h}) \cosh(k_w z_p)} \tag{4.2}$$

where h_{SD} is the standard deviation of the water depth (i.e., $[p/\rho g] + z_p$, where z_p is the elevation above the bed of the pressure sensor, p is measured pressure, g is acceleration due to gravity and ρ is water density), $\overline{h}$ is the burst-averaged water depth and k_w is the wavenumber calculated using the linear dispersion relationship with $\overline{h}$ and the mean

spectral period $\overline{T}$ (Longuet-Higgins, 1975). For each burst of test data and for each current meter, u_w and $u_{w,\text{linear}}$ were found to agree within 2%, which is taken as verification of the current-meter gains.

The drag coefficient was derived from each burst of current data using a standard technique that derives from steady-flow boundary-layer theory (e.g., Tennekes and Lumley, 1972). In a turbulent, steady, neutrally buoyant flow the vertical profile of horizontal current speed is described by the law of the wall:

$$\overline{u}_z = (\overline{u}\star/\kappa) \ln (z/z_0) \tag{4.3}$$

where $\overline{u}_z$ is the mean horizontal current speed at elevation z above the bed, κ is von Karman's constant (0.41), z_0 is the hydraulic roughness and $\overline{u}\star = (\overline{\tau}_b/\rho)^{1/2}$ is the friction velocity, where $\overline{\tau}_b$ is the time-averaged bed shear stress. The hydraulic roughness is the elevation above the bed at which the mean flow appears to vanish when the current-speed profile is extrapolated toward the bed in log $z - \overline{u}_z$ space. In the particular case of rough-turbulent flow, the hydraulic roughness is completely determined by the bed or equivalent Nikuradse roughness; in smooth-turbulent flow z_0 is related to the thickness of the viscous sublayer. In either case, the seabed drag coefficient relates the flow speed at a specified elevation above the bed to the bed shear stress. Traditionally, that elevation is 100 cm, in which case the drag coefficient is defined as $C_{100} = \overline{u}\star^2 / \overline{u}_{100}^2$, which, from (4.3), is equivalent to:

$$C_{100} = \left[\frac{\kappa}{\ln (100/z_0)} \right]^2 \tag{4.4}$$

where z_0 is in cm.

The measured current-speed profiles ($\overline{u}_z, z$) were fitted using least squares to the model $\ln (z) = (\kappa \overline{u}_z/ \overline{u}\star) + \ln (z_0)$, which is (4.3) rearranged. Hydraulic roughness was estimated from the intercept (B) of the best-fit line as $z_0 = e^B$. z_0 was then substituted into (4.4) to obtain C_{100}. The friction velocity, which will be used in parts of the following analysis, was estimated from the slope (M) of the best-fit line as $\overline{u}\star = \kappa/M$. The coefficient of explanation r^2 was evaluated for each fit of data to the model (i.e. for each burst), which Gross and Nowell (1983) related to the confidence interval around the estimate of z_0.

Eq. (4.3) applies only to the logarithmic or inner layer, which, using values typical of the Mahurangi sites in Eq. (3) of Harvey and Vincent (1977), was 1–2 m thick more than 80% of the time. We discarded from the analysis those bursts that yielded $r^2 < 0.985$, since the confidence interval around the estimate of z_0 in that case is very wide. Bursts discarded were from periods of low flow around the turn of the tide, when a well-developed logarithmic velocity profile is not expected.

b. Seabed observations

Using the marked rope, which is visible in the video footage, as a scale, each 20-m transect was divided into forty 50- by 40-cm quadrats. A frame grabber was used to
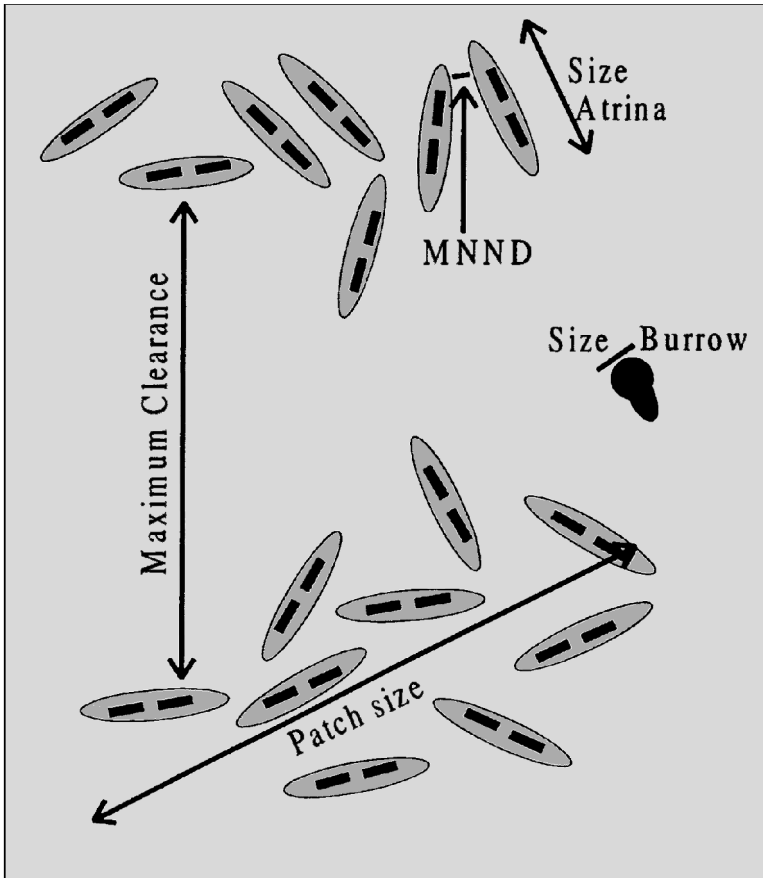
Figure 3. Definitions of parameters used to quantify seabed roughness. The ellipses represent horse mussels (the dark rectangles represent horse mussel "siphons").

generate a digital image of each quadrat from the video footage. Each digital image was examined for the presence of "roughness elements" (i.e., horse mussels, burrows and bedforms). For the horse mussels, the following parameters were measured: shell width, density, orientation, minimum nearest-neighbor distance (MNND), maximum clearance between individuals, and patch size (Fig. 3). (Protrusion of horse mussels above the seabed ["height"] was measured separately by divers.) Density is defined as the number of individual horse mussels or burrows per 50- by 40-cm quadrat (0.2 m^2). Horse mussel orientations were grouped by eight 22.5°-wide sectors (0–180° total range). For burrows, width and density were measured. There were no bedforms at any site. The spatial distribution of horse mussels at scales greater than the size of the quadrat was analyzed using Moran's *I* coefficient at 1-m lags (R Package; Legendre and Vaudor, 1991) and 1-m lag variograms (Geo-Eas; Englund and Sparks, 1991). Analyses were conducted for each "L"-shaped transect and for each arm of the transect separately.

5. Results

a. Drag coefficient

Estimates of z_0 have been averaged by phase of the tide (ebb, flood) and by site (Fig. 4). Each estimate of z_0 has an associated 95% confidence interval, which was derived using the method of Gross and Nowell (1983). The site-mean C_{100} corresponds to the site-mean z_0 (Eq. 4.4).

b. Seabed roughness elements

Densities of seabed roughness elements varied widely (Fig. 5 and Table 2); there were no horse mussels at site 4. The spatial distribution of horse mussels varied more between sites than it did within sites (Table 3), and since the scales derived from the spatial-autocorrelation analysis are all small compared to the transect length, the transect-average horse mussel densities listed in Table 2 are unbiased estimates.

6. Interpretation and discussion

a. Validity of law of the wall and dependence of drag coefficient on seabed roughness

Before attempting to relate the drag coefficient to the seabed roughness, we address two issues concerning the interpretation of the current data. Firstly, are there bursts for which the assumptions underpinning the law of the wall are invalid and therefore for which the estimate of z_0 derived from (4.3) is also invalid? Secondly, assuming that the law of the wall is valid, is it always correct to assume that z_0 (and C_{100}) is governed by only the seabed roughness elements?

Some factors could invalidate the law of the wall: effects of flow unsteadiness (e.g., Soulsby and Dyer, 1981) and effects of flow stratification by suspended sediment (e.g., Green and McCave, 1995). We summarily dismiss both of these because local acceleration of the semidiurnal tide is negligible and the water was always either clear or there was a well-mixed "washload" present with no discernible gradient in suspended-sediment concentration. We conclude that the assumptions underpinning the law of the wall are not violated and therefore it is valid to estimate z_0 from the measured velocity profiles. In that case, variation in the goodness-of-fit of the law of the wall to the data reflects random error in the current measurements, rather than any real dynamical effect that causes the velocity profile to deviate from (4.3).

There are two situations where the magnitude of z_0 (and C_{100}) would not be completely governed by the seabed roughness elements: a combined wave-current flow (e.g., Green *et al.,* 1990) and flow that was not fully rough turbulent (e.g., Chriss and Caldwell, 1984). In the first case, the mean flow above the wave boundary layer is retarded by bottom-generated turbulence and by an additional source of friction that derives from interaction of the wave and current within the wave boundary layer. In that case, z_0 is not determined uniquely by k_s, where k_s is the equivalent Nikuradse roughness of the bed. Grant and Madsen (1986) showed that in combined wave-current flow $z_0 = k_s^{1/\zeta} \delta_w^{(1-1/\zeta)}/30$, where δ_w is
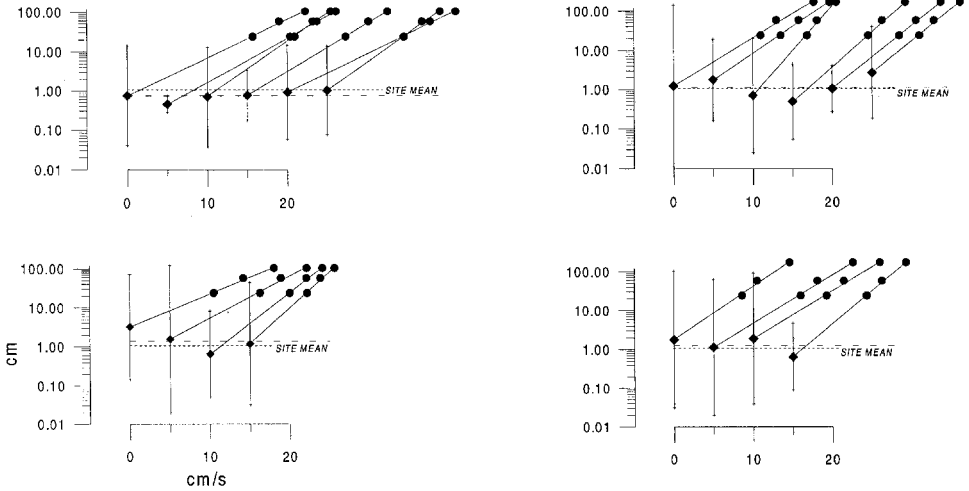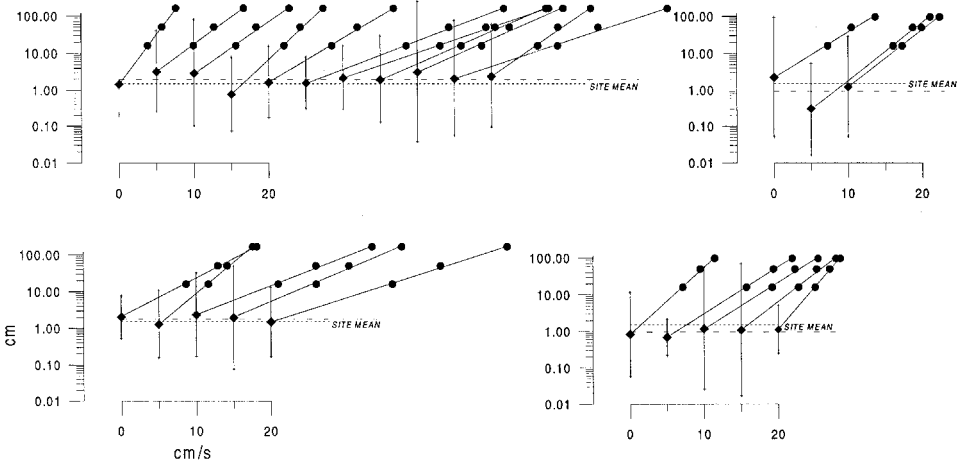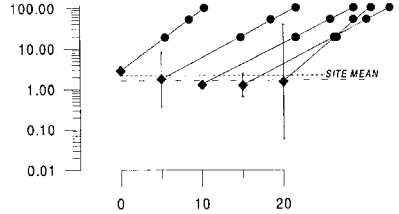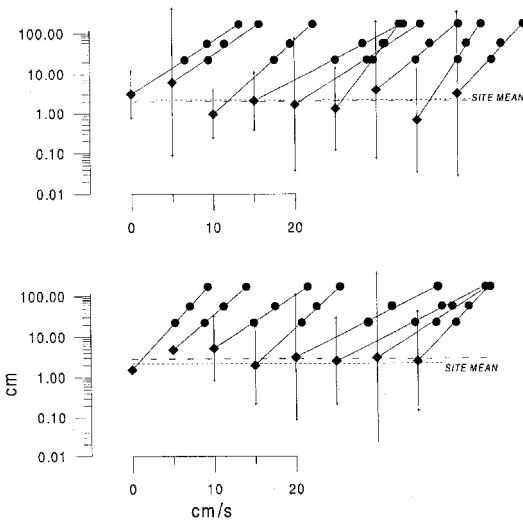
Figure 4. Velocity profiles grouped by site and by phase of the tide (ebb, flood) within sites. Each profile is plotted against a horizontal axis (cm/s) that moves to the right by 5 cm/s for each successive profile. The filled circles denote measured current speed. Each thin line is Eq. (4.3) fitted to the data. The diamonds denote z_0; the 95% confidence interval around each estimate of z_0 is shown in the standard way. The dashed line is the geometric-mean z_0 for that phase of the tide and the dotted line ("site mean") is the geometric-mean z_0 for the site. (a) Site 1, Te Kapa. (b) Site 2, Lagoon Bay. (c) Site 3, Mid-Harbour. (d) Site 4, Grants Island.
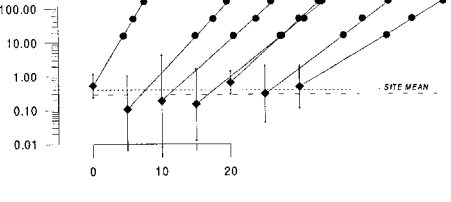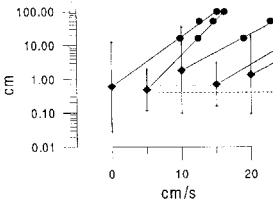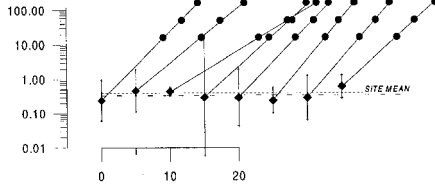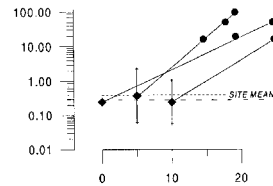
Figure 4. (Continued)

the wave boundary-layer thickness and $\zeta = u\star_t/\overline{u}\star_c$, where $\overline{u}\star_c$ is the time-averaged friction velocity above the wave boundary layer and $u\star_t$ is the sum of the time-averaged and wave-induced-maximum friction velocities. Waves do in fact penetrate to the bed from time to time, at least in the lower reaches of Mahurangi Harbour, and generate orbital
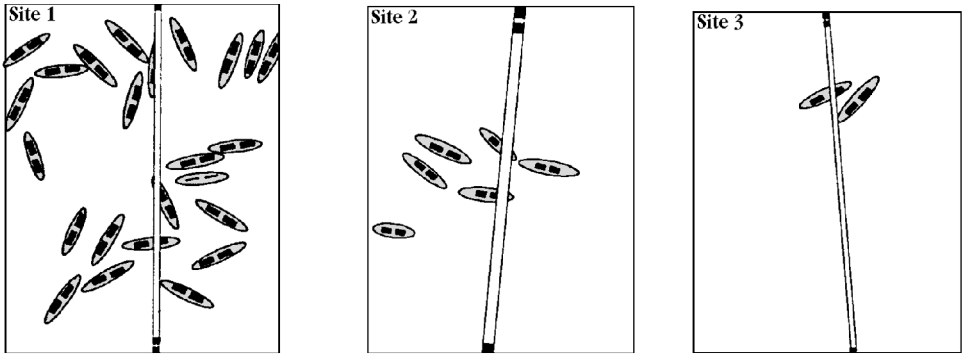
Figure 5. Schematic of horse mussel distribution at sites 1, 2 and 3, traced from actual video footage. The slim rectangle stretching the length of each panel represents the rope pegged to the seabed, which was used as a guide by the diver operating the video camera. Between the single dark patch marked on the rope and the pair of dark patches is 50 cm. Each ellipse represents a horse mussel, and the two dark rectangles on each ellipse represent horse mussel "siphons." The figure shows plan views.

speeds at the bed that are comparable with mean speeds. That was never the case, however, in the present experiment. The maximum $u_{sig,b}$, where $u_{sig,b}$ is the significant wave-orbital speed at the bed computed from the variance of the burst pressure signal using standard linear-wave theory (see, for example, Green *et al.,* 1990), was only 3 cm/s, which was measured during one burst at site 1 (Te Kapa). At all other sites and at all other times $u_{sig,b}$ was less than the value that corresponds to the noise floor of the pressure sensor, i.e. ~1 cm/s. We therefore dismiss any effect in the benthic boundary layer due to wave-current interaction.

In a rough-turbulent boundary layer under a pure current, z_0 is completely determined by the bed or equivalent-Nikuradse roughness. In that case:

$$z_0 = k_s/30 \tag{6.1a}$$

$$C_{100} = \left[\frac{\kappa}{\ln\left(100 \Big/ \dfrac{k_s}{30}\right)} \right]^2. \tag{6.1b}$$

For smooth-turbulent flow and the particular case of $\bar{u}\star\delta/v = 11.6$, where δ is the thickness of the viscous sublayer and v is the kinematic viscosity, $z_0 = v/(9\bar{u}\star)$. For all bursts, $9\bar{u}\star z_0/v \gg 1$, which indicates that the observed hydraulic roughness was much greater than the value expected had the flow been smooth turbulent. The transition to rough-turbulent flow occurs at $Re\star \approx 70$ (Daily and Harleman, 1966), where $Re\star = \bar{u}\star k_s/v$ and $Re\star$ is the roughness Reynolds number. For all bursts $Re\star \gg 70$, where $Re\star$ was evaluated as $\bar{u}\star 30z_0/v$, following (6.1a). We conclude that the boundary-layer flow was always rough turbulent. Therefore (6.1) applies and we are justified in assuming that z_0 (and C_{100}) at each site is completely governed by the seabed roughness elements alone.

Table 2. Measurements of seabed roughness elements. T1 is the 20-m transect aligned with the principal tidal axis. T2 is the 20-m transect aligned across that axis.

Type		Parameter	1 (Te Kapa)	2 (Lagoon Bay)	3 (Mid-Harbour)	4 (Grants Island)
Horse mussels						
individuals	width (cm)	T1 average	7.7	8.9	7.8	—
		T2 average	7.6	9.4	9.1	—
		overall average	7.65	9.1	8.5	—
	average height of 10 individuals (cm)		7	7	7	—
	orientation (numbers per 22.5°-sector)	T1; 10 quadrats	18, 19, 12, 15, 13, 12, 15, 13	2, 2, 3, 0, 0, 3, 4, 1	10, 16, 9, 6, 5, 6, 8, 9	—
		T2; 10 quadrats	16, 24, 41, 28, 16, 18, 26, 24	3, 3, 1, 3, 3, 4, 5, 4	7, 4, 1, 6, 7, 17, 7, 9	—
		overall average	17, 22, 26, 21, 15, 15, 21, 19	2, 2, 2, 2, 2, 3, 4, 2	8, 10, 5, 6, 6, 11, 7, 9	—
density of individuals	density (individuals per 50- × 40-cm quadrat)	T1 average	14.6	1.4	5.5	—
		T2 average	22.4	2.4	6.8	—
		overall average	19.9	1.9	6.2	—
	MNND (cm)	T1 average	0.6	172	14.1	—
		T2 average	0.5	272	4.1	—
		overall average	0.55	231	9.2	—
		overall minimum	0.1	1.0	6	—
		overall maximum	2.1	450	50	—
patches	patch size (cm)	T1 average	26.7	>50	23	—
		T2 average	32.2	>50	26	—
		overall average	30.6	>50	25	—
		overall minimum	12.8	75	10	—
		overall maximum	49	250	54	—
	maximum clearance (cm)	T1 average	18.1	190	25	—
		T2 average	19.2	292	18.8	—
		overall average	18.8	247	22	—
		overall minimum	7.4	50	3	—
		overall maximum	36.9	450	50	—
Burrows	width (cm)	T1 average	1.1	0.8	0	1.2
		T2 average	1.1	0	1.4	1.4
		overall average	1.1	0.8	1.4	1.3
	density (number per quadrat)	T1 average	0.6	1.0	0.8	0.8
		T2 average	1.3	1.2	0.2	1.8
		overall average	0.9	1.1	0.5	1.3
Bedforms			no bedforms	no bedforms	no bedforms	no bedforms
Comments						patches of dead whole cockle shells and seaweed

Table 3. Results of the spatial autocorrelation analysis of the horse mussel distribution at each of the
   three sites with horse mussels.

Site	Area	Average size of spatial structure (m)
1 (Te Kapa)	"L"-shaped transect	10
	arm of transect normal to tidal axis	3 and 10
	arm of transect parallel to tidal axis	1.5 and 10
2 (Lagoon Bay)	"L"-shaped transect	7.5
	arm of transect normal to tidal axis	7.5
	arm of transect parallel to tidal axis	7.5
3 (Mid-Harbour)	"L"-shaped transect	3
	arm of transect normal to tidal axis	3
	arm of transect parallel to tidal axis	3

b. Relationship of seabed roughness to site-mean drag coefficient

Although the boundary-layer flow encountered at the instrument tripod at any particular
time is the product of upstream roughness rather than roughness in the immediate vicinity
of the tripod, we do not have sufficient information on the state of the seabed to relate each
estimate of drag coefficient to upstream roughness at the time of each measurement.
Instead, our intention is to relate the seabed roughness at each site (as determined from the
transect survey) to the site-mean drag coefficient. We comment on the validity of this
approach at the end of this section.

The site-mean C_{100} (Fig. 6; Table 4) was smallest (0.0055) at site 4 (Grants Island), but
still twice as large as the value (0.0025) typically assumed to apply to abiotic, flat,
cohesionless beds under tidal currents. Although the bed was flat at site 4 (i.e., there were
no bedforms), it was not abiotic: the surface was covered with patches (∼1-m diam) of
dead whole cockle shells and patches of seaweed (1–2-m diam) attached to the bed. In
addition, small crab burrows were common.

The ranking of the other sites in terms of increasing site-mean C_{100} is: site 1 (0.0082),
site 2 (0.0096) and site 3 (0.0115). Bedforms were not apparent, but horse mussels were
present in each case. There were no clear differences amongst the three sites in terms of the
attributes of individual horse mussels: individuals were approximately the same width
(8–9 cm) and height (7 cm; i.e., protrusion above the seabed surface), and individuals
assumed no preferred orientations relative to the tidal flow (see Table 2). Thus it is not
possible to explain the ranking of the drag coefficients in terms of attributes of individual
horse mussels.

There were, however, differences amongst the three sites in terms of spatial distribution
of individuals. The ranking of the sites in terms of increasing density (number/quadrat) is:
site 2, site 3 and site 1 (Table 2). The ranking in terms of MNND is reversed, MNND being
roughly inversely related to density. There were also differences amongst the three sites in
terms of patch structure. At site 1, the average maximum clearance was less than the
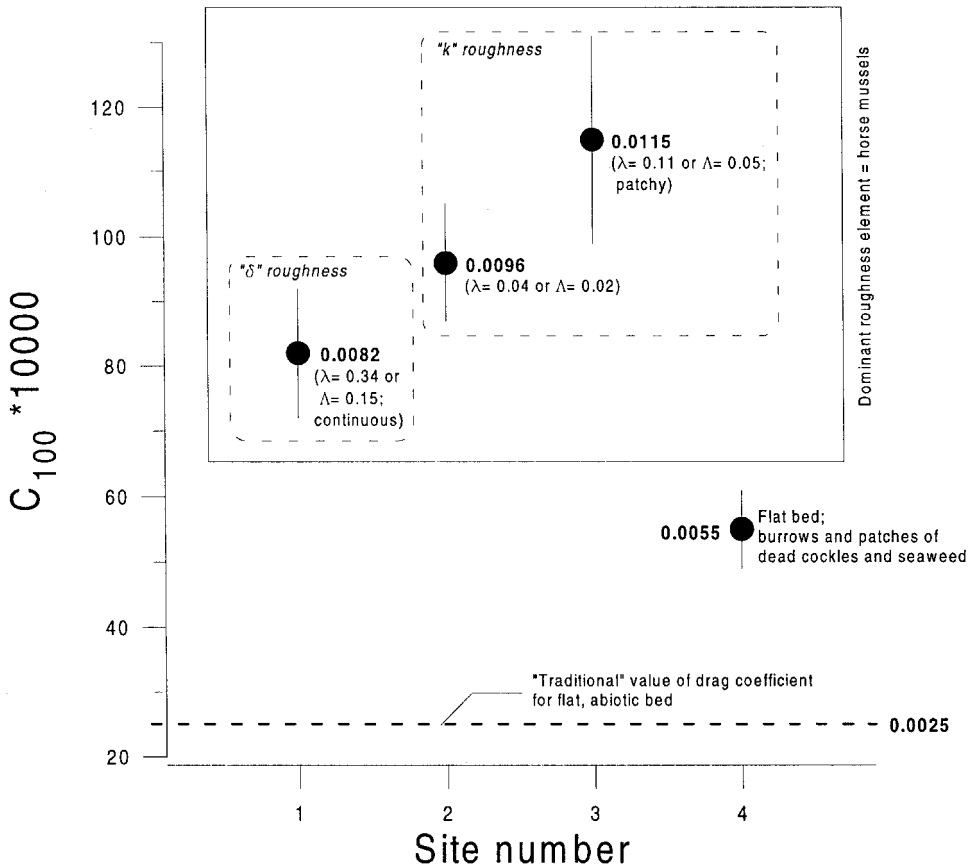
Figure 6. Site-mean C_{100} at each of the four sites.

average patch size, which implies that individuals are distributed more in a "carpet" than in patches. At site 3, the average maximum clearance was approximately the same as the average patch size, which suggests a more distinct patchiness, compared to site 1. The fact that MNND, patch size and maximum clearance are all more variable at site 3 than at site 1 (see minimum and maximum values in Table 2) also suggests a more patchy distribution at site 3, compared to site 1. At site 2, the density of individuals was so low and the maximum clearance so high that there was no obvious patchiness at all, on the scale of the quadrat.

c. Drag over horse mussels and skimming flow

For not-too-closely spaced, three-dimensional roughness elements, the equivalent-Nikuradse roughness k_s (and also z_0 through 6.1a, and C_{100} through 6.1b) is directly proportional to the product $k\lambda$, where k is the roughness-element height and λ is the areal concentration (dimensionless) of the roughness elements, which is similar to density (number of shells/quadrat) or abundance, but takes into account exposure of the individual

Table 4. The site-mean drag coefficient is shown with plus-or-minus standard error. k is the roughness element height; d is the roughness-element width in the dimension transverse to the mean flow; D is the mean element spacing; λ is the areal concentration of roughness elements, $\lambda = kd/D^2$. "Type" refers to the roughness types identified by Perry *et al.* (1969) and Wooding *et al.* (1973); k_s is the bed or Nikuradse roughness (Eq. 6.1a) and m is the constant of proportionality in Eq. (6.2). H and L are the height and length, respectively, of the ripples that, according to Eq. (6.4) and assuming ripple steepness 0.1, would generate hydraulic roughness equal to site-mean z_0.

	Site-mean C_{100} and standard error	k cm	d cm	D cm	λ	Λ	type	Site-mean z_0 cm	k_s cm	m	H, L cm
1 (Te Kapa)	0.0082 ± 0.0010	7	4.8	10	0.34	0.15	"δ" $[\lambda > \lambda_c]$	1.1	32	—	14, 140
2 (Lagoon Bay)	0.0096 ± 0.0009	7	5.4	32	0.04	0.02	"k" $[\lambda < \lambda_c, D = O(k)]$	1.5	46	176	19, 190
3 (Mid Harbour)	0.0115 ± 0.0016	7	5.1	18	0.11	0.05	"k" $[\lambda < \lambda_c, D = O(k)]$	2.2	66	86	28, 280
4 (Grants Island)	0.0055 ± 0.0006	—	—	—	—	—	"k, D" $[\lambda < \lambda_c, D \gg k]$	0.4	12	—	5, 50

roughness elements to the flow (Koloseus and Davidian, 1966). Given that horse mussels are approximately the same height and width at sites 1, 2 and 3, we therefore expect the drag coefficient to be highest at site 1 where the horse mussel density is greatest, which is not the case.

The anomalously low drag coefficient at site 1 can be explained in terms of skimming flow. Morris (1955) showed that there is a critical areal concentration of roughness elements (λ_c) which coincides with the onset of mutual sheltering of roughness elements from the flow. For $\lambda > \lambda_c$, the space between the adjacent roughness elements contains a stable eddy which aids in the establishment of skimming flow (Wooding *et al.,* 1973); in effect the shear layer rolls on top of the field of stable eddies, thus reducing the drag. Wooding *et al.* termed roughness that behaves in that way "δ" roughness, and noted that for flat-topped "δ" roughness, the drag coefficient tends to a smooth-wall value as $\lambda \to 1$. Figure 1 of Wooding *et al.,* in which some of Koloseus and Davidian's (1966) data are reproduced, shows a range of values for λ_c, from ~ 0.1 for rectangular bars to ~ 0.2 for spheres. To test whether the data are consistent with skimming flow, we estimated λ for each site, as follows. Wooding *et al.* (1973) defined the areal concentration of roughness elements as $\lambda = A_r/S$, where A_r is the frontal area of the roughness element and S is the specific area or average area of flat surface per roughness element. When the roughness-element shape is invariant, which we assume to be the case for horse mussels, $\lambda = kd/D^2$, where d is the projection of the roughness-element width in the plane transverse to the mean flow and D is the mean element spacing (Fig. 7). To estimate λ for each site, we set k as the average individual mussel height (see Table 2); we computed an average d for each site by distributing the average size (Table 2) across the eight orientation sectors as given in Table 2; and we estimated D by assuming mussels were uniformly distributed throughout the quadrat at the average density (Table 2). In that way, λ for site 2 was estimated as 0.04, for site 3 as 0.11 and for site 1 as 0.34 (Table 4). If we assume that the decrease in drag coefficient at site 1 compared to site 3 is indeed due to skimming flow, then we can infer
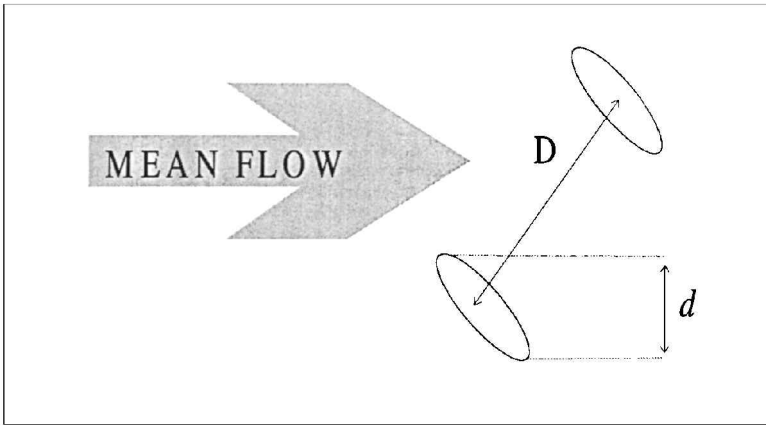
Figure 7. Definition of *d*, the projection of the horse mussel width in the plane transverse to the mean
flow, and *D*, the mean horse mussel spacing, used to evaluate λ, the areal concentration of horse
mussels. The figure shows a plan view; the ellipses represent horse mussels.

that, for horse mussels ~8–9 cm wide protruding above the seabed ~7 cm, $0.11 < \lambda_c < 0.34$, or $\lambda_c \approx 0.2$. Since that value for λ_c is very similar to the values given in Wooding *et al.*'s Figure 1, it is plausible that the decrease in drag coefficient at site 1 relative to site 3 was due to skimming flow and that the horse mussels at site 1 were therefore behaving as "δ" roughness. The Mahurangi data are also consistent with Nowell and Church's (1979) data from depth-limited boundary layers in a flume. Nowell and Church found that the total boundary resistance increased to a maximum at roughness density Λ equal to 0.1, and then declined for roughness densities beyond that value, where Λ is defined as NA_e/A_t and N is the number of roughness elements, A_e is the plan area of individual roughness elements and A_t is the total bed area. Following Morris (1955) and Perry *et al.* (1969), Nowell and Church attributed the decline to skimming flow. Thus, the critical roughness density for the onset of skimming flow Λ_c was ~0.1. By setting N in each quadrat to the overall average density of individual shells (Table 2), A_e as the overall average width (Table 2) multiplied by 2.0 cm (which is the typical bivalve thickness at the top of the shell) and A_t as 2000 cm² (i.e., the quadrat area), we estimate Λ for site 2 as 0.02, for site 3 as 0.05, and for site 1 as 0.15 (Table 4). Thus, Λ for site 1 is greater than Nowell and Church's value for Λ_c, which strengthens our inference of skimming flow and associated drag reduction at site 1. It is conceivable, and worthy of further attention because of the implication to boundary-layer dynamics over bivalve reefs, that the vertical momentum imparted to the very-near-bed flow through the nonsiphonal filtering activity of the horse mussels acts to stabilize the boundary layer. Siphonal excurrents, which are more concentrated than nonsiphonal excurrents and known to interact with the turbulent boundary layer (e.g., O'Riordan *et al.,* 1995), may have a different effect on the boundary-layer dynamics.

For $\lambda < \lambda_c$, the eddy between elements is unstable and is shed into the shear flow. In that case, the turbulence structure is scaled to the roughness height, which results in the

previously mentioned relationship:

$$k_s = mk\lambda. \tag{6.2}$$

For $D = O(k)$, where D is the horizontal distance between roughness elements, there is not space enough for reattachment of the flow between roughness elements; Perry *et al.* (1969) termed this case "k" roughness (or "wake interaction" flow). For $\lambda < \lambda_c$ and $D \gg k$, the flow can reattach between roughness elements, in which case (6.2) still holds, but the smooth wall between the elements makes a positive contribution to the total drag. Perry *et al.* termed this case "k, D" roughness (or "isolated roughness" flow).

Wooding *et al.*'s (1973) Figure 1 gives some sample values for m, including 0.88 for rectangular bars in air and 0.22 for spheres in air. Combining (6.2), (6.1a) and (6.1b), the drag coefficient is related to m by:

$$C_{100} = \left[\frac{\kappa}{\ln (3000/mk\lambda)} \right]^2 \tag{6.3}$$

which is valid only for $\lambda < \lambda_c$. We used the observed site-mean drag coefficient from sites 2 and 3 in (6.3) to estimate m for horse mussels (Table 4).

It is not possible to ascertain whether our two estimates of m (one from site 2 and one from site 3) are representative of a single "true" value, in which case the variation in the estimates of m is due to random measurement error, or whether the two estimates reflect a real trend in m. We can conclude at this stage only that $m \approx 100$ for the natural beds of horse mussels and await further experiments to elucidate any variation in m.

Soulsby (1983) gave the following equation, derived from Wooding *et al.* (1973), for z_0 associated with ripples of height H and length L in steady flow:

$$z_0 = 2.0H(H/L)^{1.4}. \tag{6.4}$$

Eq. (6.4) was used to calculate the size of the ripples equivalent to each site-mean z_0, assuming that ripples were of equilibrium steepness $H/L = 0.1$. In terms of hydraulic roughness, the horse mussel beds in Mahurangi Harbour are equivalent to rather large bedforms (Table 4), which suggests that horse mussel beds are quite effective at dissipating mean-flow energy. Energy dissipation by bed friction depends roughly on the drag coefficient multiplied by the cube of the free-stream current speed. Thus, assuming that the free-stream flows at the two sites are the same speed, approximately twice as much energy will be dissipated by friction over the horse mussels at site 3 (site-mean $C_{100} = 0.0115$) compared to site 4 with no horse mussels (site-mean $C_{100} = 0.0055$). Compared to the "traditional" abiotic seabed ($C_{100} = 0.0025$), energy dissipation will be approximately four times greater at site 3 over horse mussels (again, assuming similar current speeds).

The fact that onset of skimming flow is expressed only in terms of a critical bed geometry implies that, once initiated, skimming flow will persist throughout the tidal cycle as the mean flow waxes and wanes. The essentially invariant drag coefficient at site 1 (Fig. 4a) is consistent with that implication. Skimming flow has interesting implications for

both the ecology of horse mussels and the influence of bivalves on infaunal communities and surficial sediment characteristics. The stable eddies characteristic of a patch of "δ" roughness horse mussels may become depleted of food and/or dissolved gases, which would have a deleterious effect on individuals, cf. Frechette *et al.* (1989), who showed that food supply to the bed is increased by the increase in turbulent transport caused by the enhanced hydraulic roughness associated with the mussel *Mytilus edulis*. At the same time, skimming flow over the "δ" roughness will provide shelter for individuals from hydrodynamic forces. On the other hand, horse mussels distributed at concentrations less than the critical value may benefit from increased turbulent diffusion (Frechette *et al.,* 1989), but at the cost of greater exposure to the forces generated by the fluid shear. Changes in infaunal composition are often attributed to modifications in flow that influence the settlement and dispersal of larvae and post-larvae (e.g., Eckman, 1983). Our analysis demonstrates one way that boundary-layer structure may be radically changed by biogenic surface roughness, which therefore may have a concomitant effect on the infaunal composition.

d. Upstream roughness

Our analysis has been founded on relating site-mean drag coefficient to seabed roughness in the immediate vicinity (within 20 m) of the current-meter array, even though we acknowledged previously that boundary-layer flows are the product of upstream roughness, not local roughness. Our approach therefore will be valid only if the local seabed roughness as determined from each transect survey is representative of the upstream roughness. Since the site-mean drag coefficient is actually a tidal average and the tide is essentially rectilinear at each site, the "upstream roughness" in our case must correspond to the roughness of an ellipse-shaped area centered on each site. Hence, for the transect roughness to be representative of the upstream roughness, the seabed in that imaginary ellipse must be unchanging through time and uniform over space. Since bedforms, which could conceivably change shape and/or size over the tidal cycle (e.g., Dyer, 1980), were secondary to the horse mussel communities, which should not change significantly over the duration of the experiment (one week), the first condition (i.e., roughness constant through time) is satisfied. In order to address the second condition, we first need to estimate the size of the imaginary ellipse at each site, which we do in the following by examining how boundary-layer flow responds to change in roughness.

In the most extreme case, an internal boundary layer, which can be treated as a separate and almost independent boundary layer (Antonia and Luxton, 1971), develops downstream of a discontinuous change in roughness. The thickness of the internal boundary layer, δ_{IBL}, grows in the downstream direction, x, as:

$$\delta_{IBL} = z_{0,d}[0.75 - 0.03 \ln (z_{0,d}/z_{0,u})](x/z_{0,d})^{0.8} \qquad (6.5)$$

(Elliot, 1958), where $z_{0,d}$ is the hydraulic roughness downstream ($x > 0$) of the change and $z_{0,u}$ is the hydraulic roughness upstream ($x < 0$) of the change. Eq. (6.5) can be used to calculate x_{200}, which is the distance needed for the internal boundary layer to grow to a thickness of 200 cm following a change of roughness. x_{200} was calculated for sites 1, 2 and

3, where $z_{0,u}$ was set to 0.4 cm and $z_{0,d}$ was set to the actual hydraulic roughness for each site in question. The upstream value of 0.4 cm is the same as the hydraulic roughness at site 4, which has been chosen as a "background" roughness, i.e., devoid of the influence of horse mussels. 200 cm is the approximate height of the tripod. For site 1, x_{200} was 16 m, for site 2 it was 19 m and for site 3 it was 25 m. Thus, the internal boundary layer that would grow over a typical horse-mussel patch sited within featureless seabed would completely enclose the current-meter array within only about 20 m of the edge of the patch. $x_{\bar{h}}$, which is the distance needed for the internal boundary layer to grow to a height equal to the mean water depth, can also be calculated from (6.5). Addressing the same changes in roughness as above and using the mean water depths in Table 1, for site 1 $x_{\bar{h}}$ was 39 m, for site 2 it was 61 m and for site 3 it was 43 m. Although the internal boundary layer grows quite rapidly, the bed shear stress immediately downstream of the roughness change overshoots before more slowly returning to an equilibrium value. Antonia and Luxton (1971) found that mean-flow integral parameters, including the Clauser friction factor, reach equilibrium values at a distance less than 20 equilibrium boundary-layer thicknesses downstream of a roughness change in a steady flow. Assuming that the equilibrium boundary-layer thickness at each site is equal to the mean water depth, and addressing yet again the same changes in roughness, equilibrium would be attained approximately 80 m downstream of the roughness change at site 1, 100 m downstream at site 2 and 60 m downstream at site 3. Such calculations give an appreciation of the distances over which boundary-layer flows in Mahurangi Harbour adjust when flowing over patches of horse mussels studding otherwise featureless seabed. From these calculations, we estimate that uniform seabed roughness extending for an upstream distance of about 100 m is reasonable in the Mahurangi Harbour to ensure a fully developed boundary-layer flow. Our experimental sites were all situated in areas of the harbor where the seabed was deemed to be homogeneous for at least 150 m on either side. Thus, the second condition above (i.e., roughness uniform over the entire upstream area) is satisfied, and we therefore conclude that the seabed roughness as determined from each transect survey is indeed representative of the upstream roughness that is associated with the site-mean drag coefficient. We conclude that our basic approach, viz. relating a site-mean drag coefficient to a local seabed roughness, is valid. Our statement that experimental sites were situated in homogeneous areas is made on the basis of past scan-sonar surveys and diver observations and is therefore not rigorous; future work should incorporate replicate sampling to provide a more rigorous test of such propositions.

Although the key process inferred from the Mahurangi data set is the action of eddies at the scale of individual horse mussels, in order for the site-mean drag coefficient to be affected, such eddies must act over the entire upstream area, which extends for $\sim$100 m parallel to the principal tidal axis. Thus, our results demonstrate a link between benthic biota and flow dynamics at the 100-m "mesoscale."

7. Conclusions

The site with the highest areal concentration of horse mussels, site 1, had the lowest drag coefficient amongst the three sites with horse mussels. Since the areal concentration of

horse mussels at site 1 was higher than typical critical values cited by Wooding *et al.* (1973) for inducing skimming flow over spheres and rectangular bars, we hypothesize that the anomalously low drag coefficient there was due to the presence of stable eddies in the space between horse mussels inducing a skimming flow. Direct observations of turbulence are required to verify the hypothesis. Eddies between horse mussels at sites 2 and 3 are shed into the flow, in which case turbulence structure is scaled to the roughness height. In that case, the Nikuradse or bed roughness is $mk\lambda$ and the constant of proportionality, m, we estimate from the data as being $\sim$100. Thus, in steady, neutrally buoyant, rough-turbulent boundary-layer flow, the drag coefficient of beds of natural horse mussels with areal concentration $<\sim$0.2 is given by:

$$C_{100} = \left[\frac{\kappa}{\ln(3000/mk\lambda)}\right]^2$$

where $m \approx 100$. Skimming flow ensues over horse mussels $\sim$8–9 cm wide and $\sim$7 cm high at $\lambda = \sim$0.2. The Mahurangi data set has an important implication for the interpretation of ecological experimental data: since boundary-layer flow over "δ" roughness elements is not similar to flow over "k" or "k, D" roughness, it may not be valid to extrapolate experimental findings from one flow type to the other.

APPENDIX

Notations

A_e	plan area of roughness element
A_r	frontal area of roughness element
A_t	total bed area
B	intercept (fitting of wall law to velocity profile)
C_{100}	drag coefficient referenced to flow at 100 cm above bed
d	projection of roughness-element width in plane transverse to mean flow
D	mean roughness-element spacing
D_g	mean grain size
f	frequency
g	gravitational acceleration
h_{SD}	standard deviation of water depth
$\overline{h}$	mean water depth

H	ripple height
k	roughness-element height
k_s	equivalent Nikuradse roughness
k_w	gravity-wave wavenumber
L	ripple length
m	constant of proportionality in Eq. (6.2)
M	slope (fitting of wall law to velocity profile)
MNND	minimum nearest-neighbor distance
N	number of roughness elements
p	pressure
r^2	coefficient of explanation
$Re_\star$	roughness Reynolds number
S	average area of flat surface per roughness element
$\overline{T}$	mean spectral period
u_w	standard deviation of wave-orbital speed (estimated from current data)
$u_{sig,b}$	significant wave-orbital speed at the bed
$u_{w,\text{linear}}$	standard deviation of wave-orbital speed (estimated from pressure data)
$\overline{u}_z$	mean current speed at elevation z above the bed
$\overline{u}_\star$	time-averaged friction velocity
$\overline{u}_{\star c}$	time-averaged friction velocity above the wave boundary layer
$u_{\star t}$	sum of time-averaged and wave-induced-maximum friction velocities
x	distance downstream of a step change in hydraulic roughness
x_{200}	distance needed for an internal boundary layer to grow to a thickness of 200 cm following a step change in hydraulic roughness
$x_{\overline{h}}$	distance needed for an internal boundary layer to grow to a thickness equivalent to the mean water depth following a step change in hydraulic roughness
z	elevation above the bed
z_p	pressure-sensor elevation above the bed
z_r	reference elevation
z_u	current-meter elevation above the bed
z_0	hydraulic roughness
$z_{0,u}$	hydraulic roughness upstream of a step change in roughness
$z_{0,d}$	hydraulic roughness downstream of a step change in roughness
ε	power spectrum of current speed
δ	thickness of viscous sublayer
δ_w	thickness of wave boundary layer
δ_{IBL}	thickness of internal boundary layer
κ	von Karman's constant
λ	areal concentration of roughness elements
λ_c	critical areal concentration of roughness elements for onset of skimming flow

Λ	roughness-element density
Λ_c	critical roughness-element density for onset of skimming flow
v	kinematic viscosity of seawater
ρ	density of seawater
$\overline{\tau}_b$	time-averaged bed shear stress
ζ	$u\star_t / \overline{u}\star_c$

REFERENCES

Antonia, R. A. and R. E. Luxton. 1971. The response of a turbulent boundary layer to a step change in surface roughness. Part 1. Smooth to rough. J. Fluid Mech., *48,* 721–761.

Butman, C. A., M. Frechette, W. R. Geyer and V. R. Starczak. 1994. Flume experiments on food supply to the blue mussel *Mytilus edulis* L. as a function of boundary-layer flow. Limnol. Oceanogr., *39,* 1755–1768.

Cacchione, D. A., D. E. Drake, W. D. Grant and A. J. Williams, III. 1983. Variability of seafloor roughness within the Coastal Ocean Dynamics Experiment (CODE) region. WHOI Tech. Rep. 83-25, Woods Hole Oceanographic Institute, Woods Hole, MA, 44 pp.

Chriss, T. M. and D. R. Caldwell. 1982. Evidence for the influence of form drag on bottom boundary layer flow. J. Geophys. Res., *87,* 4148–4154.

—— 1984. Universal similarity and the thickness of the viscous sublayer at the ocean floor. J. Geophys. Res., *89,* 6403–6414.

Cummings, V. J., S. F. Thrush, J. E. Hewitt and S. J. Turner. 1998. The influence of the pinnaid bivalve *Atrina zelandica* (Gray) on benthic macroinverterbrate communities in soft-sediment habitats. J. Exp. Mar. Biol. Ecol., (in press).

Daily, J. W. and D. R. F. Harleman. 1966. Fluid Dynamics, Addison-Wesley, Reading, Massachusetts, 454 pp.

Dietrich, W. D. 1982. Flow, Boundary Shear Stress, and Sediment Transport in a River Meander, Ph.D. Dissertation, University of Washington, Seattle, 261 pp.

Dyer, K. R. 1980. Velocity profiles over a rippled bed and the threshold of movement of sand. Estuar. Coast. Mar. Sci., *10,* 181–199.

Eckman, J. E. 1983. Hydrodynamic processes affecting benthic recruitment. Limnol. Oceanogr., *28,* 241–257.

—— 1985. Flow disruption by an animal-tube mimic affects sediment bacterial colonization. J. Mar. Res., *43,* 419–435.

Eckman, J. E., A. R. M. Nowell and P. A. Jumars. 1981. Sediment destabilization by animal tubes. J. Mar. Res., *39,* 361–374.

Elliot, W. P. 1958. The growth of the atmospheric internal boundary layer. Trans. Am. Geophys. Union, *39,* 1048–1054.

Englund, E. and A. Sparks. 1991. Geo-Eas 1.2.1, Geostatistical Environment Assessment Software. User's Guide. U.S. Environmental Protection Agency, 600/8-9/1008, Las Vegas.

Frechette, M., C. A. Butman and W. R. Geyer. 1989. The importance of boundary-layer flows in supplying phytoplankton to the benthic suspension feeder *Mytilus edulis L.* Limnol. Oceanogr., *34,* 19–36.

Gambi, M. C., A. R. M. Nowell and P. A. Jumars. 1990. Flume observations on flow dynamics in *Zostera marina* (eelgrass) beds. Mar. Ecol. Prog. Ser., *61,* 159–169.

Grant, W. D., L. F. Boyer and L. P. Sanford. 1982. The effects of bioturbation on the initiation of motion of intertidal sands. J. Mar. Res., *40,* 659–677.

Grant, W. D. and O. S. Madsen. 1979. Combined wave and current interaction with a rough bottom. J. Geophys. Res., *84,* 1797–1808.

—— 1982. Movable bed roughness in unsteady oscillatory flow. J. Geophys. Res., *87,* 469–481.

—— 1986. The continental-shelf bottom boundary layer. Ann. Rev. Fluid Mech., *18,* 265–305.

Grant, W. D., A. J. Williams, III, and S. M. Glenn. 1984. Bottom stress estimates and their prediction on the northern California continental shelf during CODE-1: The importance of wave-current interaction. J. Phys. Oceanogr., *14,* 506–527.

Green, M. O. and I. N. McCave. 1995. Seabed drag coefficient under tidal currents in the eastern Irish Sea. J. Geophys. Res., *100* (C8), 16057–16069.

Green, M. O., J. M. Rees and N. D. Pearson. 1990. Evidence for the influence of wave-current interaction in a tidal boundary layer. J. Geophys. Res., *95* (C6), 9629–9644.

Gross, T. F. and A. R. M. Nowell. 1983. Mean flow and turbulence scaling in a tidal boundary layer. Cont. Shelf Res., *2,* 109–126.

Harvey, J. G. and C. E. Vincent. 1977. Observations of shear in near-bed currents in the southern North Sea. Estuar. Coast. Mar. Sci., *5,* 715–731.

Huntley, D. A. and D. G. Hazen. 1988. Seabed stresses in combined wave and steady flow conditions on the Nova Scotia continental shelf: Field measurements and predictions. J. Phys. Oceanogr., *18,* 347–362.

Hurd, C. L., C. L. Stevens, B. Laval, G. A. Lawrence and P. J. Harrison. 1997. Visualization of seawater flow around morphologically distinct forms of the giant kelp *Macrocystis integrifolia* from wave-sheltered and exposed sites. Limnol. Oceanogr., *42,* 156–163.

Kamphuis, J. W. 1974. Determination of sand roughness for fixed beds. J. Hydr. Res., *12,* 193–203.

Koloseus, H. J. and J. Davidian. 1966. Free-surface instability correlations, and roughness-concentration effects on flow over hydrodynamically-rough surfaces. United States Geological Survey Water-Supply Paper 1592-C.

Legendre, P. and A. Vaudor. 1991. The R Package: Multidimensional Analysis, Spatial Analysis. Departement de Sciences Biologiques, Universitie de Montreal, Montreal, Canada, 142 pp.

Longuet-Higgins, M. S. 1975. On the joint distribution of the period and amplitudes of sea waves. J. Geophys. Res., *80,* 2688–2694.

Madsen, T. V. and E. Warnke. 1983. Velocities of currents around and within submerged aquatic vegetation. Arch. Hydrobiol., *97,* 389–394.

Morris, H. M. 1955. A new concept of flow in rough conduits. Trans. Am. Soc. Civil Eng., *120,* 373–398.

Nielsen, P. 1983. Analytical determination of nearshore wave height variation due to refraction, shoaling and friction. Coastal Eng., *7,* 233–251.

Nowell, A. R. M. and M. Church. 1979. Turbulent flow in a depth-limited boundary layer. J. Geophys. Res., *84,* 4816–4824.

Nowell, A. R. M., P. A. Jumars and J. E. Eckman. 1981. Effects of biological activity on the entrainment of marine sediments. Mar. Geol., *42,* 133–153.

O'Riordan, C. A., S. G. Monismith and J. R. Koseff. 1993. A study of concentration boundary-layer formation over a bed of model bivalves. Limnol. Oceanogr., *38,* 1712–1729.

—— 1995. The effect of bivalve excurrent jet dynamics on mass transfer in a benthic boundary layer. Limnol. Oceanogr., *40,* 330–344.

Perry, A. E., W. H. Schofield and P. N. Joubert. 1969. Rough wall turbulent boundary layers. J. Fluid Mech., *37,* 383–413.

Peterson, C. H., H. C. Summerson and P. B. Duncan. 1984. The influence of seagrass cover on population structure and individual growth rate of a suspension-feeding bivalve, *Mercenaria mercenaria.* J. Mar. Res., *42,* 123–138.

Rhoads, D. C. and L. F. Boyer. 1982. The effects of marine benthos on physical properties of sediment, *in* Animal-Sediment Relationships, P. L. McCall and M. J. S. Teresz, eds., Plenum, New York, 3–57.

Shashar, N., S. Kinane, P. L. Jokiel and M. R. Patterson. 1996. Hydromechanical boundary layers over a coral reef. J. Exp. Mar. Biol. Ecol., *199,* 17–28.

Smith, J. D. and S. R. McLean. 1977. Spatially averaged flow over a wavy surface. J. Geophys. Res., *82,* 1735–1746.

Soulsby, R. L. 1983. The bottom boundary layer of shelf seas, *in* Physical Oceanography of Coastal and Shelf Seas, B. Johns, ed., Elsevier, Amsterdam, 189–266.

—— 1990. Tidal-current boundary layers, *in* The Sea, *9,* B. LeMehaute, and D. M. Hanes, eds., John Wiley and Sons, New York, 523–566.

Soulsby, R. L. and K. R. Dyer. 1981. The form of the near-bed velocity profile in a tidally accelerating flow. J. Geophys. Res., *86,* 8067–8074.

Sternberg, R. W. 1968. Friction factors in tidal channels with differing bed roughness. Mar. Geol., *6,* 243–260.

—— 1970. Field measurements of the hydrodynamic roughness of the deep-sea boundary. Deep-Sea Res., *17,* 413–420.

Tennekes, H. and J. L. Lumley. 1972. A First Course in Turbulence, MIT Press, Cambridge, MA, 300 pp.

Warwick, R. M., A. J. McEvoy and S. F. Thrush. 1997. The influence of *Atrina zelandica* Gray on nematode diversity and community structure. J. Exp. Mar. Biol. Ecol., *214,* 231–247.

Wheatcroft, R. A. 1994. Temporal variation in bed configuration and one-dimensional bottom roughness at the mid-shelf STRESS site. Cont. Shelf Res., *14,* 1167–1190.

Whitehouse, R. J. S. and T. J. Chesher. 1994. Seabed Roughness in Tidal Flows. A Review of Existing Measurements. Report SR 360, HR Wallingford, Wallingford, U.K., 24 pp.

Wiberg, P. L. and D. M. Rubin. 1989. Bed roughness produced by saltating sediment. J. Geophys. Res., *94,* 5011–5016.

Wilkinson, R. H. 1986. Variation of roughness length of a mobile sand bed in a tidal flow. Geo-Mar. Lett., *5,* 231–239.

Wooding, R. A., E. F. Bradley and J. K. Marshall. 1973. Drag due to irregular arrays of roughness elements of varying geometry. Boundary-Layer Meteorol., *5,* 285–308.

Yaglom, A. M. 1979. Similarity laws for constant-pressure and pressure-gradient turbulent wall flows. Ann. Rev. Fluid Mech., *11,* 505–540.